JOURNAL OF SPACECRAFT AND ROCKETS
Vol. 45, No. 2, March–April 2008

Design, Analysis, and Testing of Mars Tumbleweed Rover Concepts

Jamie L. Wilson,* Andre P. Mazzoleni,† and Fred R. DeJarnette‡
North Carolina State University, Raleigh, North Carolina 27695
Jeffrey Antol§ and Gregory A. Hajos§
NASA Langley Research Center, Hampton, Virginia 23681
and
Christopher V. Strickland¶
NASA Wallops Flight Facility, Wallops Island, Virginia 23337

DOI: 10.2514/1.31288

A Mars Tumbleweed rover is a spherical, wind-driven, planetary rover. Compared with conventional rovers, a tumbleweed rover can travel farther faster and gain access to areas such as valleys and chasms that previously were inaccessible. This paper presents design, mathematical modeling, computer simulation, and testing of various tumbleweed rover concepts. In particular, we present wind-tunnel data indicating that a box-kite configuration represents a promising tumbleweed rover design, we show that a working box-kite–type tumbleweed can be constructed, and we show that center of mass variation shows promise as the basis of a tumbleweed rover navigation system.

Nomenclature

${}^{O}\mathbf{a}_{\text{c.m.}/O}$	=	acceleration of the center of mass of the system with respect to the inertial frame, ft/s^2
Cd	=	drag coefficient
${}^{O}\frac{\mathrm{d}}{\mathrm{d}t}{}^{O}\mathbf{h}_{B,\text{sys}}$	=	time derivative with respect to inertial frame of system angular momentum about B
m_{TOT}	=	total mass of the system, lbm
$m_{1_{A,B}}$	=	small submass located along the positive and negative $\mathbf{i}_B$ axes, respectively, lbm
$m_{2_{A,B}}$	=	small submass located along the positive and negative $\mathbf{j}_B$ axes, respectively, lbm
$m_{3_{A,B}}$	=	small submass located along the positive and negative $\mathbf{k}_B$ axes, respectively, lbm
R	=	radius of the tumbleweed, ft
Re	=	Reynolds number
V	=	fluid speed, ft/s
${}^{O}\mathbf{v}_{B/O}$	=	velocity of point B with respect to the inertial frame, ft/s
${}^{O}\mathbf{v}_{\text{c.m.}/O}$	=	velocity of the center of mass of the system with respect to the inertial frame, ft/s
$x_{1_{A,B}}$	=	distance from the center of mass of the system to the submasses $m_{1A,B}$, ft
$y_{2_{A,B}}$	=	distance from the center of mass of the system to the submasses $m_{2A,B}$, ft
$z_{3_{A,B}}$	=	distance from the center of mass of the system to the submasses $m_{3A,B}$, ft
α	=	angle of attack
$\tau_{B,\text{sys}}$	=	sum of all external torques acting on the system about point B
ω_x	=	angular velocity of the tumbleweed rover about the $\mathbf{i}_B$ axis, rad/s
ω_y	=	angular velocity of the tumbleweed rover about the $\mathbf{j}_B$ axis, rad/s
ω_z	=	angular velocity of the tumbleweed rover about the $\mathbf{k}_B$ axis, rad/s

I. Introduction

THE idea of the Mars Tumbleweed rover was first introduced in 1998 when NASA researchers noticed that the Mars Pathfinder Lander traveled farther bouncing on its airbags than the Sojourner rover traveled throughout its 90 day mission. Thus was born the Mars Tumbleweed, a spherical, wind-driven, planetary rover. A second origin of the Mars Tumbleweed involves experiments related to NASA's testing of large inflatable wheels, as reported by Lorenz in the book, *Spinning Flight* [1]. (Another related concept is the "Mars Ball" developed by the University of Arizona in the 1980s [1].) Unlike conventional rovers, the tumbleweed can travel farther faster and gain access to areas such as valleys and chasms that are inaccessible to traditional wheeled rovers. The tumbleweed's ability to travel long distances makes it an excellent candidate for surface survey missions, such as large area-mapping of the Mars environment. The tumbleweed is also significantly less expensive than traditional rovers, which permits multiple tumbleweeds to be deployed across the planet's surface. Unlike previous Mars missions, the loss of a single tumbleweed will not result in mission failure.

After recognizing the tumbleweed's potential for Mars exploration, NASA's Jet Propulsion Laboratory (JPL) started development of a lightweight "beach-ball" robotic vehicle that could be driven by wind and/or internal electric power. These rovers were conceived for carrying scientific instruments across rocky terrain on Mars and are intended to move faster, weigh less, and consume less power than wheeled robotic vehicles used in planetary exploration. JPL's concept encompassed both single and double ball rovers [2]. In 2002, Wang and Yang [3] presented an analytical model for the mobility of a tumbleweed ball, where the shape and gravity center of the ball and the area of contact between the ball and ground were determined as functions of the internal pressure. Conditions of the sliding and rolling motion of the ball on slopes under wind loads were

Received 8 May 2007; revision received 24 September 2007; accepted for publication 24 September 2007. Copyright © 2007 by Andre P. Mazzoleni. Published by the American Institute of Aeronautics and Astronautics, Inc., with permission. Copies of this paper may be made for personal or internal use, on condition that the copier pay the $10.00 per-copy fee to the Copyright Clearance Center, Inc., 222 Rosewood Drive, Danvers, MA 01923; include the code 0022-4650/08 $10.00 in correspondence with the CCC.

*Graduate Student, Mechanical and Aerospace Engineering, 2601 Stinson Drive. Student Member AIAA.

†Associate Professor, Mechanical and Aerospace Engineering, 2601 Stinson Drive. Associate Fellow AIAA.

‡Professor, Mechanical and Aerospace Engineering, 2601 Stinson Drive. Fellow AIAA.

§Aerospace Engineer, Architectures, Missions, and Science Branch, MS 462.

¶Aerospace Engineer, Mechanical Systems Branch, MS 548. Member AIAA.

also quantified and numerical results were provided. Lorenz proposed the Mars Tumbleweed rover as an ideal platform for a magnetometer, to better understand the broad, parallel stripes with alternating magnetic polarity above the Martian surface [4]. Kuhlman [5] discussed additional capabilities of the tumbleweed, such as performing autonomous long duration surveys over large areas on Mars. The tumbleweed could, for example, map the presence of liquid water as a function of depth using simple low mass and low power instruments and an onboard positioning system. Tumbleweed rovers have been proposed to explore Martian gully features as well as other surface areas that are unreachable by traditional wheeled rovers [6–11]. Other researchers have begun focusing on specific instrumentation for the Mars Tumbleweed, such as deployment devices and solar power sources [12]. There are three main structural concepts being explored in relation to the tumbleweed: inflatable, structured, and a combination of the two. The inflatable designs are derived from the Mars Pathfinder Lander airbags. The structured designs are derived from toys such as the box kite or the Hoberman Sphere™, and a cross between inflatable and structured designs is similar to the Zorb™, which is a hard structured ball inside an inflatable ball.

In this paper, we present our approach to developing a path to achieve a successful Mars Tumbleweed rover mission; this approach consists of three parts: 1) conduct wind-tunnel tests to examine different methods of producing drag which will propel a wind-driven tumbleweed rover; 2) build a Tumbleweed Earth Demonstrator based on one of the promising concepts identified during the wind-tunnel testing; and 3) develop a mathematical model and perform computer simulations to investigate the possibility of using a system which can change the center of mass location of a tumbleweed rover for navigation purposes.

II. Wind-Tunnel Tests of Evolved Mars Tumbleweed Concepts

As stated previously, a Mars Tumbleweed rover is a concept for an exploration vehicle that would derive mobility through use of the winds on Mars. The tumbleweed would conduct random sampling of the surface and atmosphere, traveling long distances over broad regions of the Martian surface. NASA Langley Research Center (LaRC) and North Carolina State University (NCSU) have developed several concepts for tumbleweed rovers and have been studying the aerodynamics of these concepts through wind-tunnel testing and computational fluid dynamics analysis. We present here an overview of the latest wind-tunnel tests, which were conducted in the LaRC Basic Aerodynamic Research Tunnel (BART). Various configurations of four tumbleweed concepts, seen in Fig. 1, were tested to determine and assess their drag characteristics. Descriptions of the models are provided as well as an overview of the BART facility and the strain gage balance used in the test. A description of the test methodology and the resulting data are presented followed by conclusions drawn from the results [13].

The goal of this research, using deployable open structure concepts, is to achieve drag coefficients (Cd) greater than that of a simple sphere (0.5) to minimize the size of the tumbleweed and/or increase the instrument mass capability. Thus, we have initiated a threefold, evolutionary test strategy to measure the drag characteristics and better understand the tumbleweed concepts: 1) in the freestream, at the appropriate Reynolds number (Re); 2) on the surface, in a simulated Mars boundary layer at the appropriate Reynolds number; and 3) in a Mars relevant environment, at the appropriate temperature, pressure, and density. The tests discussed in this paper cover the first category, freestream testing. The associated wind-tunnel models, test configurations, and the balance data are presented next. The freestream drag coefficient was used as a starting point to assess the aerodynamic properties of the various tumbleweed concepts. Because the vehicles are operating on the surface of Mars and not in the freestream, the boundary layer will be critical in the performance of the tumbleweed. The Texas Tech University atmospheric boundary layer (ABL) wind tunnel was employed to examine several tumbleweed concepts in a simulated Martian atmospheric boundary layer [14]. A comparison was made between the freestream drag coefficient and the boundary layer drag coefficient to determine the extent to which the atmospheric boundary layer affects drag. Wind induced rolling moments were not examined in the tests due to funding and schedule limitations.

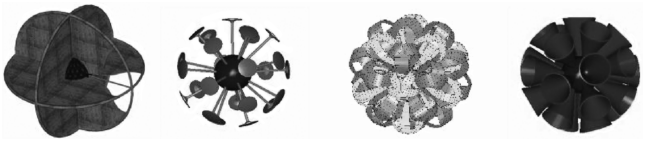

Fig. 1 NASA LaRC tumbleweed concepts, from left to right: box kite, dandelion, eggbeater dandelion, and tumble cup.

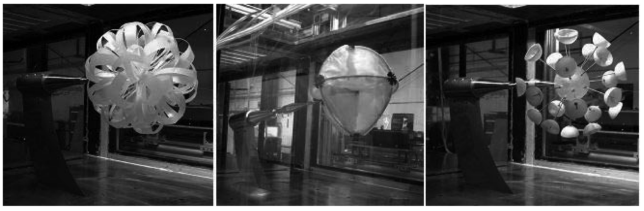

Fig. 2 Evolved LaRC tumbleweed concepts in the BART test section (from left to right, eggbeater dandelion, cloth sail box, and cup-pad dandelion).

A. Model Design

To match the expected Reynolds numbers for the surface of Mars ($Re = 50,000$–$125,000$) from average winds to storm gusts, small-scale models were needed as well as very low wind-tunnel test speeds to meet the expected Reynolds numbers. Models on the order of 1 ft in diameter were selected to ease manufacturing, to simplify model changes, and to match the test section criteria of the wind tunnel. Three evolved tumbleweed designs were selected for the tests seen in Fig. 2. The first dandelion concept employed a curved beam structure, named the eggbeater dandelion. The box kite model used cloth sails as opposed to an earlier test, which used solid "sail" panels, and the cup-pad dandelion used deeply cupped pads as opposed to the slightly cupped pads of the original dandelion model from earlier tests. The eggbeater dandelion and the cloth sail box kite models were new developments, while the cup-pad dandelion used many components from the original dandelion model.

1. Eggbeater-Dandelion Model

The eggbeater-dandelion tumbleweed was derived from the original dandelion tumbleweed concept (depicted in Fig. 1)—a central core with radial spoke legs that "provide load bearing mechanical isolation for the core and mechanical support for drag producing surfaces" [10]. A nonlinear impact dynamics analysis of the original dandelion demonstrated that radial legs would encounter structural buckling problems at the required impact velocities [15]. The straight spoke legs of the dandelion were thus replaced with legs of a curved beam design, with each leg resembling an eggbeater or whisk, hence the name "eggbeater dandelion" seen in Fig. 3. The width of each ribbon on each leg is tapered radially from the core attachment point to provide additional drag producing surface area. Three- and five-ribbon legs were combined to allow interlocking of the ribbons of adjacent eggbeater legs to enable more drag surface area without leg-to-leg physical interference. To maintain spherical symmetry, the configuration included 32 legs with attachment points coincident with the vertices of the two largest platonic solids, the dodecahedron (20 vertices) and the icosahedron (12 vertices).

The core design chosen to accomplish the compounded dodecahedron/icosahedron vertices attach points for the wind-tunnel model was a truncated icosahedron. A truncated icosahedron is essentially a soccer ball with planar patches. The centers of the 20 hexagon patches of a soccer ball correspond with the dodecahedron vertices and the centers of the 12 pentagon patches of a

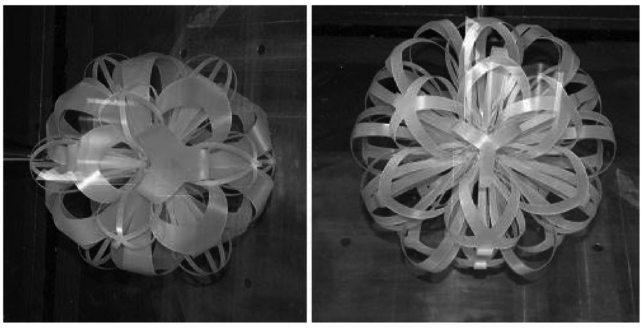

Fig. 3 Eggbeater-dandelion models.

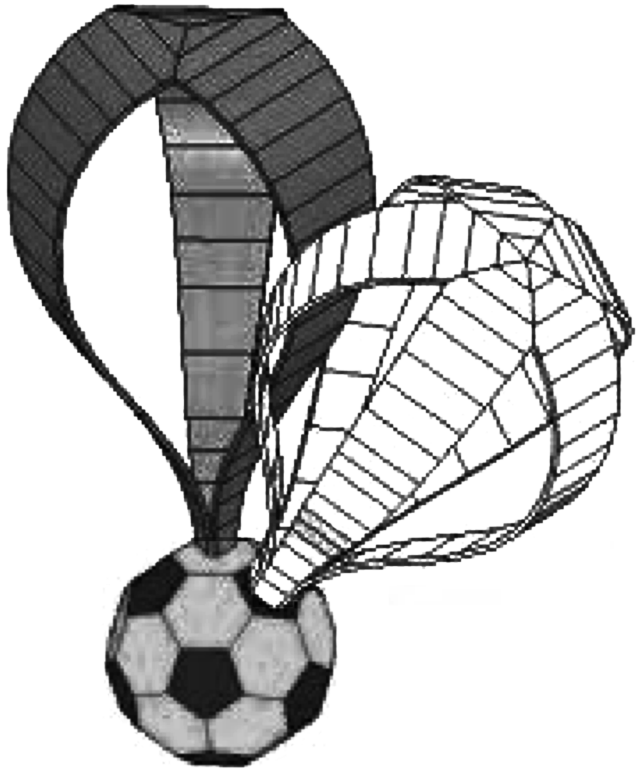

Fig. 4 Eggbeater-dandelion truncated icosahedron core with a three- and a five-ribbon leg installed.

soccer ball correspond with the icosahedron vertices. Figure 4 depicts the general core scheme of the eggbeater-dandelion tumbleweed wind-tunnel model with one three-ribbon leg and one five-ribbon leg installed. Each of the 12 pentagon patches has five 0.25-in. wide by 0.026-in. thick by 0.45-in. deep (in the radial direction) slots to accept the five tabs of the five-ribbon legs seen in Fig. 5. Similarly, the 20 hexagonal patches of the core have three slots each to accept the three tabs of the three-ribbon legs. A 1/4–20-in. screw thread insert was installed in the core to provide for attachment to the wind-tunnel sting assembly. The cores for the wind-tunnel models were manufactured from SI-10 material by the NASA LaRC model shop using the Viper^{TM} stereolithography (SL) system from 3-D Systems.

The legs were cut from a 0.02-in. thick woven fiberglass reinforced epoxy sheet by Custom Cutting Technologies, Inc., as per Fig. 5. The three-ribbon and five-ribbon legs were cut at three different taper angles. The smallest taper angle for each was called "low," the middle angle was called "medium," and the largest taper angle was called "high." The surface areas of three-ribbon low and five-ribbon low are approximately equal. Similarly, the three- and five-ribbon medium areas are approximately equal as are both highs. This was done to create a through flow path with no "easy" route. It was hypothesized that flow tripping and reformation would lead to

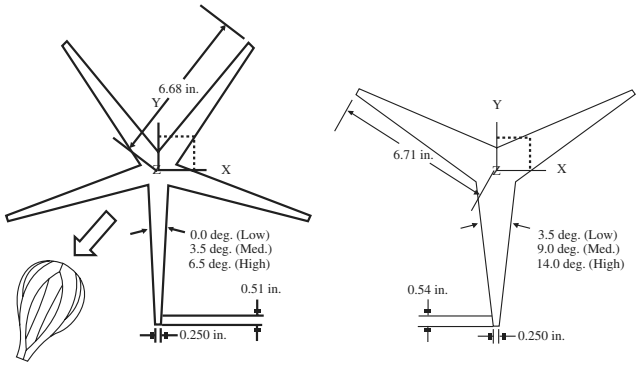

Fig. 5 Drawing for the manufacture of three- and five-ribbon eggbeater-dandelion legs.

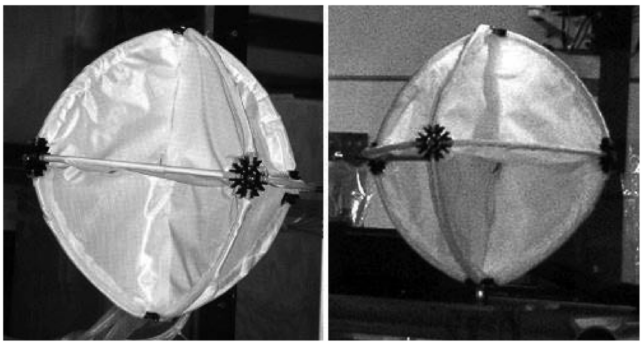

Fig. 6 Cloth sail box-kite model.

drag coefficients greater than that of a solid sphere. The primary test configurations combined the "low-to-low," "medium-to-medium," and "high-to-high" taper angle three- and five-ribbon legs. Because the tabs of the legs were held in the slots of the core by friction and/or interference fit, secondary testing was done by removing the legs from the primary test configuration and recombining 1) the three-ribbon lows with the five-ribbon mediums, 2) the three-ribbon mediums with the five-ribbon highs, and 3) the three-ribbon highs with the five-ribbon lows.

2. Cloth Sail Box-Kite Model

A commercially available watercraft radar reflector, consisting of three orthogonal circular aluminum plates, was used as the box-kite model in earlier wind-tunnel tests, but a new box-kite model was constructed for the tests presented in this paper to examine a more realistic configuration with cloth sails, instead of the rigid panels, as would be employed in the Martian tumbleweed. It was anticipated that an increased drag effect would be observed due to "billowing" effects provided by the cloth sails.

The cloth sail box-kite model was constructed from common, off-the-shelf hobby materials seen in Fig. 6. The outer ring frame structure of the model was composed of three orthogonal hoops of K'nex^{TM} tubing and associated connectors. The sails were created using 0.75 oz/yd rip-stop nylon covering each quadrant section of each hoop. A central core was fabricated using a 2-in. wooden sphere and connected radially to the hoop "nodes" using no. 4 threaded rods. A 1/4–20 in. screw thread insert was also installed in the wooden sphere to provide for attachment to the wind-tunnel sting assembly.

3. Wooden Box-Kite Model

A lightweight wooden model was constructed of 1/64th in. (0.4-mm) thick birch plywood to reduce the mass of the box-kite model from that of the aluminum model used in the previous tests. The three orthogonal 12-in. diam circular panels were glued and taped into position as seen in Fig. 7. The wooden box-kite model used the same sting adaptor as the aluminum model, providing a consistent

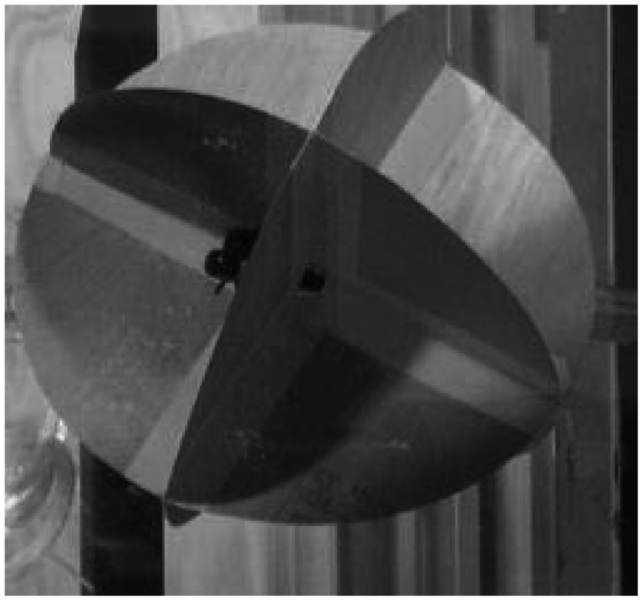

Fig. 7 Wooden box-kite model.

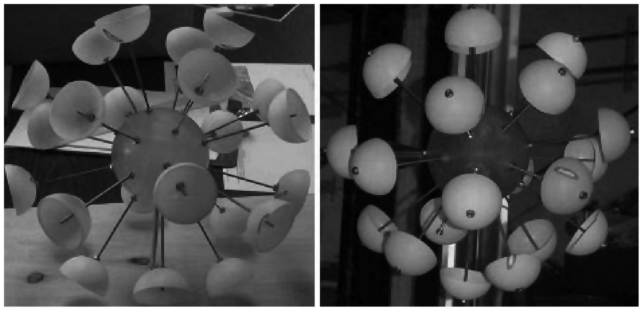

Fig. 8 Cup-pad dandelion model, outward facing pads (left) and inward facing pads (right).

mounting position and orientation between the two models. It was anticipated that variations in the test results between the aluminum model and the wood model would be a result of the minor difference in diameter and flexibility induced dynamic effects (flutter).

Before installation in the wind tunnel, both of the box-kite models were subjected to winds in excess of 150% of the planned test speeds to examine the flutter and to verify the structural integrity of the models. The cloth sail and wooden box-kite models are more flexible than the aluminum model and flutter was experienced during the verification test but no signs of damage were detected.

4. *Cup-Pad Dandelion Model*

In an effort to optimize the design of the dandelion tumbleweed, open hemispherical end pads (cups), known for having a high drag coefficient, were examined. Two variations were constructed (see 8); however, only the configuration with the open end of the pads facing out from the center of the tumbleweed was tested due to time constraints. The hemispherical cup has a long history of use in anemometers and the aerodynamic characteristics of such a cup are well known in axial flow. One objective of this test was to examine the combined effects of these cups in spherical arrays as used by the dandelion tumbleweed.

The cup pads were constructed of oversized ping-pong balls (2 1/8-in. diameter) which were cut in half and mounted on no. 4–40 threaded rods of the 24-stem stereolithography hollow sphere core (outer diameter of 4 in.). Jam nuts and washers held the hemispheres in position on the rods. The outside diameter of each configuration was kept to 12 in. to allow comparison with the other 12-in. diam tumbleweed models.

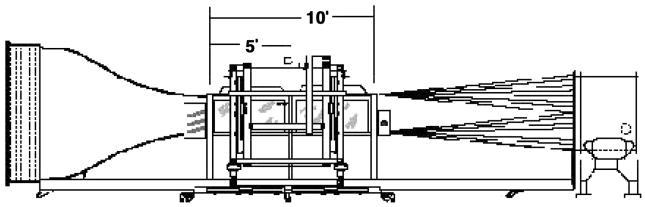

Fig. 9 The basic aerodynamic research tunnel (BART) at NASA Langley Research Center.

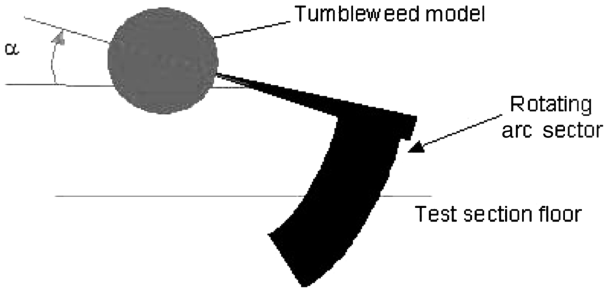

Fig. 10 Test configuration—rotating arc sector.

B. Wind-Tunnel Facility and Test Configuration

The basic aerodynamic research tunnel at NASA Langley was selected due to the low Reynolds number requirements of the project. NASA-Langley's BART tunnel shown in Fig. 9 is a subsonic, low-turbulence, open-return wind tunnel with a test section 10 ft long and a cross-section dimension of 28 in. high and 40 in. wide. The test section consists of two 5-ft cells, with large Plexiglas windows that provide access for flow visualization studies. The model angle of attack and data acquisition is remotely controlled using LabView™ software. The maximum velocity in the test section is 185 ft/s, which yields a Re/ft of 1.4×10^6. Aerodynamic loads were determined by the use of a model balance outfitted with internal strain gauges.

The model support system (depicted in Fig. 10) traveled through angles of attack (AOA) from $-5 < \alpha < +25$ deg using a rotating arc sector.

A NASA LaRC balance, Strain Gage Balance 734, was used for the tests. A more sensitive balance was desired but the pitching moment limit was exceeded due to the model weight and the length of the sting attachment. Balance characteristics for the 734 balance are shown in Table 1.

C. Wind-Tunnel Test

Smoke visualization tests were performed first to examine the flow as it traveled through and around select models. This was followed by strain gage balance tests, which were conducted at tunnel wind speeds of approximately 20 and 40 ft/s. The Reynolds number at 20 ft/s ($Re = 123,000$) is within the range of interest for wind gusts measured on Mars by the Viking Lander; however, at this speed the fan of the BART is near its lowest operating speed and produces somewhat unsteady flow through the test section. Therefore, tests were also conducted at 40 ft/s, which is at the higher end of the range of interest (Martian dust storms), to achieve a reliable steady flow.

1. *Smoke Visualization*

A standard theatrical smoke/fogger machine was positioned on a stand in front of the BART inlet screen, allowing the flow to converge on the front of the model in the first test section. The balance was not installed during the smoke visualization tests due to the oil buildup that could occur on the strain gages; so only photographic data were recorded for these tests (still pictures were taken during each test). Wind-tunnel speeds for the smoke test were conducted at 11, 20, and 25 ft/s and only the egg beater dandelion models were tested in the smoke visualization seen in Fig. 11.

Table 1 NASA LaRC strain gage balance 734 characteristics

Component	Calibration load range, lb or in. · lb	Calibration load range, N or N · m	Full scale output, mV/V	Sensitivity constant, lb/mV/V or in. · lb/mV/V	Sensitivity constant, N · m/mV/V or N/mV/V	Accuracy % full scale, 95% conf.
Normal	25.0	111.206	1.189	21.0200	93.5016	0.06
	−25.0	−111.206	——	——	——	——
Axial	5.0	22.241	1.122	4.4550	19.8168	0.12
	0.0	0.000	——	——	——	——
Pitch	40.0	4.519	1.264	31.6580	3.5769	0.07
	−40.0	−4.519	——	——	——	——
Roll	10.0	1.130	1.603	6.2370	0.7047	0.16
	−10.0	−1.130	——	——	——	——
Yaw	20.0	2.260	1.303	15.3530	1.7347	0.09
	−20.0	−2.260	——	——	——	——
Side	10.0	44.482	1.317	7.5910	33.7665	0.18
	−10.0	−44.482	——	——	——	——

2. Strain Gage Balance Test

After each model was mounted to the sting, three tares were performed to determine the loads on the balance due to the model weight at the different angles of attack in order to be subtracted from the test data. Once the tare data were loaded into the LabView™ software, the tunnel fan was started and the 20 ft/s flow tests were initiated. The models were then swept from negative to positive angles of attack while stopping at every degree interval to record data. Every test was completed 3 times so that an average data set could be generated and to ensure that constant data were being recorded. The tests were then repeated at the 40 ft/s wind speed.

D. Wind-Tunnel Data

After each model was tested at 20 and 40 ft/s, the data were compiled, checked for consistency, and the averages of all three tests were plotted. All data corresponding to the slower test speed of 20 ft/s are plotted using dashed lines while the faster 40 ft/s data are plotted using solid lines. The plot of drag coefficient versus the angle of attack for the dandelion and box-kite tumbleweed models and for calibration spheres (4-in. sphere and 12-in. globe) is shown in Fig. 12. The dandelion and spheres were tested at 20 and 40 ft/s wind speeds, while the box kite could only be tested at 20 ft/s due to the instability of the lightweight models at higher test speeds. The plot of drag coefficient versus the angle of attack for the eggbeater-dandelion models is shown in Fig. 13. No negative angles of attack were tested for any of the eggbeaters because the models were heavier than others and would overload the balance.

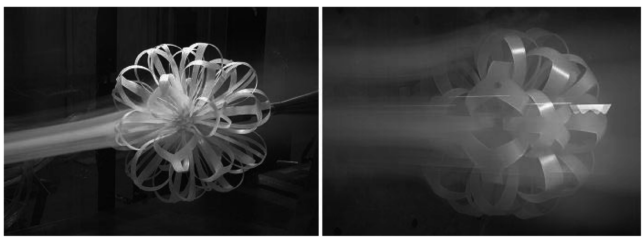

Fig. 11 Smoke visualization test of eggbeater-dandelion configurations.

The "AC" and "AE" designation (Fig. 13) of the eggbeater-dandelion tumbleweeds refers to the "clocking" on the sting of Fig. 14. At zero angle of attack, the symmetry axis of the windward five-ribbon leg would be parallel to the oncoming wind-tunnel wind direction. For the AC tests, the eggbeater-dandelion tumbleweed was clocked such that one of the neighboring three-ribbon legs was due North. For the AE tests, the eggbeater-dandelion tumbleweed was clocked such that one of the neighboring five-ribbon legs was due North.

E. Discussion of Wind-Tunnel Results

The slower test speed of 20 ft/s for each set of tests shows widely varying values for drag coefficient as compared with the higher test speed. Because the lower speed is very near the operating limit of the tunnel, it was determined that the flow must be unsteady in the test

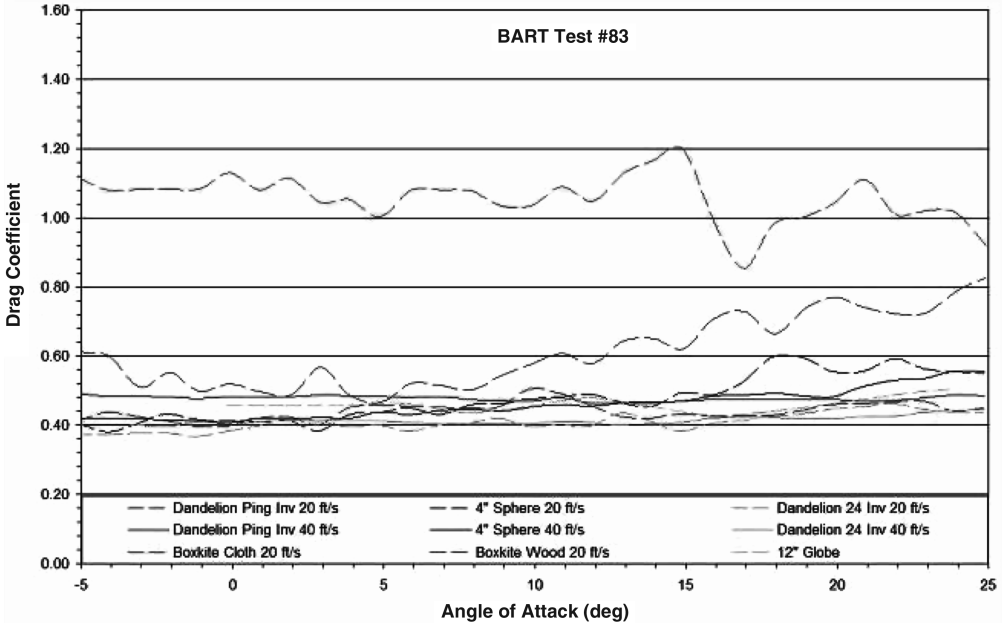

Fig. 12 Plot of drag coefficient versus angle of attack for dandelion, box kite, and calibration spheres.

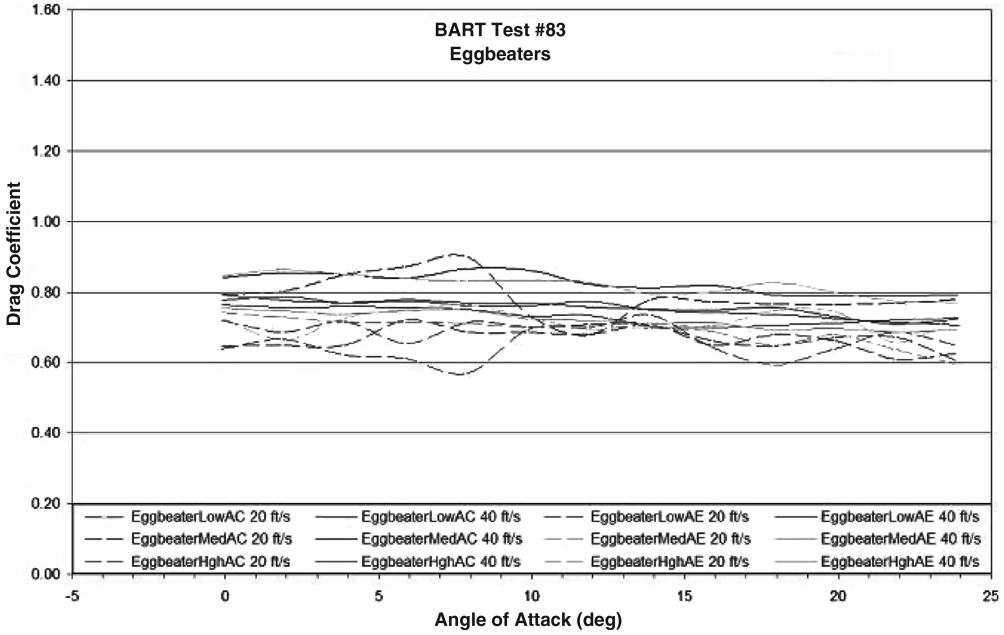

Fig. 13 Plot of drag coefficient versus angle of attack for eggbeater-dandelion configurations.

Fig. 14 Eggbeater-dandelion naming convention for clocking.

section and therefore should only be used as a qualitative comparison with the other tests. All quantitative comparisons and conclusions will be based on the higher and steadier 40 ft/s test speeds.

The calculated drag coefficient for both dandelion models, inverted pads and inverted ping, shown in Fig. 12, fall in the same range as the 4-in. and 12-in. calibration spheres. This result indicates that the spoke models may not have a better drag than an equivalent sphere regardless of the drag shapes mounted at the ends. Note that this result is inconsistent with the previous wind-tunnel tests of the baseline dandelion tumbleweed [16]; this may be due to the unsteady flow issues in the BART. Additional test cases are needed to resolve the discrepancy, but were not conducted due to funding and schedule limitations. The box-kite models show a higher drag coefficient but the models could only be tested at the slower, unsteady, speed of 20 ft/s. The box-kite sail demonstrates a higher drag coefficient than the box-kite wood and the rigid box kite from the prior test. This was partially due to the different orientation (i.e., flat plate) of the cloth sail box kite and the billowing effect of a flexible fabric sail, which aids in adding drag to the box-kite shape.

All variations of the eggbeater-dandelion design exhibit drag characteristics that change by no more than 5% for all models tested. The drag coefficient of the eggbeaters is higher than a sphere of the same size (Cd of 0.6 to 0.85 for the eggbeater vs $Cd \approx 0.5$ for a sphere). The most likely reason for this, as hypothesized, is that the wind flow is being tripped (disturbed), reformed, and tripped again as the wind flow passes through the open structure of the eggbeater-dandelion tumbleweed. Also, as hypothesized, increasing the ribbon taper angle (which increases ribbon area) increased the drag coefficient to an inflection point at which the drag coefficient starts to decline. This decline probably occurs when the path of least wind flow resistance is around as opposed to through the eggbeater dandelion, thereby approaching spherelike drag coefficients. It should be noted that even higher drag coefficient numbers are expected if the presently ridged ribbons were replaced with cloth sail ribbons. This effect was observed for the box kite due to billowing of the cloth sails.

Data from the tests indicate that the box kite has the best overall drag coefficient of the wind-tunnel models tested (Cd of 0.8–1.2). Out of the four tumbleweed concepts shown in Fig. 1, the data from these tests indicate that the box kite and the tumble cup show the most promise from a coefficient of drag standpoint ($Cd > 1.0$). Based on these results, we decided to design and construct a "Tumbleweed Earth Demonstrator" (or TED) based on the box-kite design. A description of our work on developing a Tumbleweed Earth Demonstrator is found in the next section.

III. Design, Construction and Testing of a Tumbleweed Earth Demonstrator

Because the wind-tunnel testing indicates that the box-kite concept is a promising concept for a Mars Tumbleweed rover, it was decided that it would be important to design and construct a TED based on the box-kite concept, to start identifying the critical design issues associated with an eventual Mars mission which would use box-kite–type tumbleweed rovers. To date, three generations of TEDs have been developed.

A. Design

The first Tumbleweed Earth Demonstrator was designed and constructed by students at North Carolina State University with guidance from engineers at NASA Langley. It became known as the TEDI and was the first in a succession of TEDs. The TEDI was constructed as a one-third scale (6.6-ft diam) prototype of the tumbleweed rover. The TEDI had a rigid outer structure, with orthogonal sails to create drag and therefore propel the TED. It had a fixed instrument core in the center of the structure and solar panels on the sails.

After initial testing of the TEDI, it was evident that the next generation of TEDs would need to have a larger sail area to enable testing to be done on days when winds were light. This new design became known as TEDII. The TEDII had a diameter of 9.9 ft, and the increased sail area enabled the structure to be propelled in lighter

winds. However, given TEDII's increased size and weight, the outer structure began to buckle under rolling loads. TEDII's design had also been improved from the previous TEDI by adding a sail retraction and deployment system and a gimbaled modular instrument system with solar panels on the upper face. However, the sail area was only decreased by approximately 40% by this retraction design, and during testing retraction was shown to slow the TED down but was not able to stop it completely from rolling. Also, the outer members buckled when rolling, interfering with the gimbal design and keeping it from working correctly.

It became evident after testing that a new sail retraction and deployment system would be needed if stop/start capabilities were desired. Also, a more rigid structure would be needed to preserve the spherical shape and protect the gimbaled modular instrument system inside. These requirements, again resulted in another generation of Tumbleweed Earth Demonstrators called TEDIII. The TEDIII's outer structure was made of PVC piping and provided enough rigidity to exhibit a structured Mars Tumbleweed's capabilities. The TEDIII also had a new sail retraction and deployment system and a new gimbaled modular instrument system (MIS). The new sail retraction system decreased the sail area by almost 100% which effectively stopped the TEDIII. To start rolling again the sails needed only to be redeployed. The gimbaled MIS was also redesigned to be smaller, stronger, and more efficient.

B. Construction

1. *Tumbleweed Earth Demonstrator I*

The outer structure of the TEDI had a basic box-kite configuration. It consisted of three, 3-in. diam, orthogonal hoops made of a carbon fiber/Kevlar hybrid. The hoops were covered in a flexible sail material with an instrument core located in the center. Additional hoops, without sail material, were added to assist the rolling properties. The prototype instrument core was a 10-in. diam, stereolithography core, created by Fineline Prototyping Incorporated. It contained two removable hatches to access the core interior and attached to the sails by Velcro. Figure 15 shows the TEDI with the orthogonal sails and instrument core incorporated.

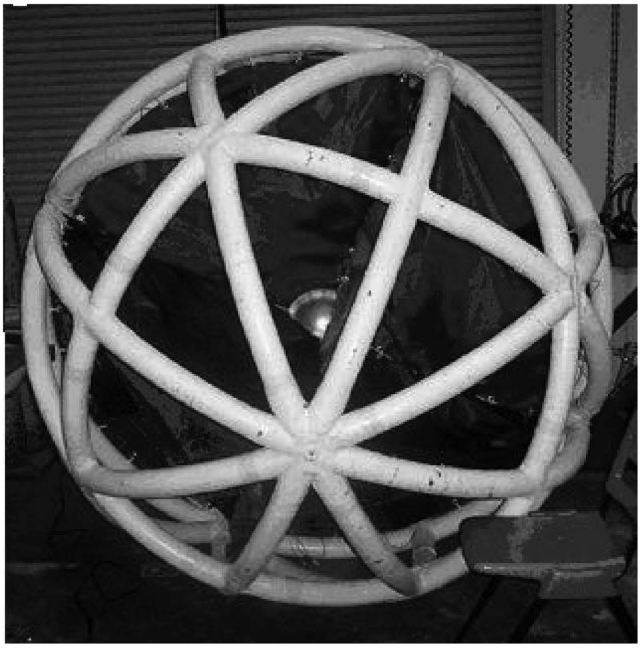

Fig. 15 Tumbleweed Earth Demonstrator I.

2. *Tumbleweed Earth Demonstrator II*

The outer structure of the TEDII was made up of a 2-in. carbon fiber/Kevlar hybrid sleeve. The hybrid sleeve was chosen for its light weight, strength, and durability. The structure was composed of 24 main members, 2 hubs, and 1 center ring. Each hub had 12 appendages, with 30 deg separating each. The inner structure consisted of six hollow aluminum struts that attach the double gimbal system (DGS) seen in Fig. 16 to the outer structure. The DGS, allowed the MIS to remain upright while rolling. The DGS consisted of three rings and was constructed of a 1-in. carbon fiber sleeve with a blue foam core. The MIS was designed not only to protect the instruments and power source, but also to allow the instruments to be easily accessed and modified. The MIS box contained all of the instruments including a 3-axis accelerometer, pressure and temperature sensors, a magnetometer, an anemometer, a global positioning system (GPS) unit, and a video camera. The MIS had a removable front panel and shelf system to easily access and modify the instrumentation. The completed TEDII, with sails, DGS, and MIS is shown in Fig. 17.

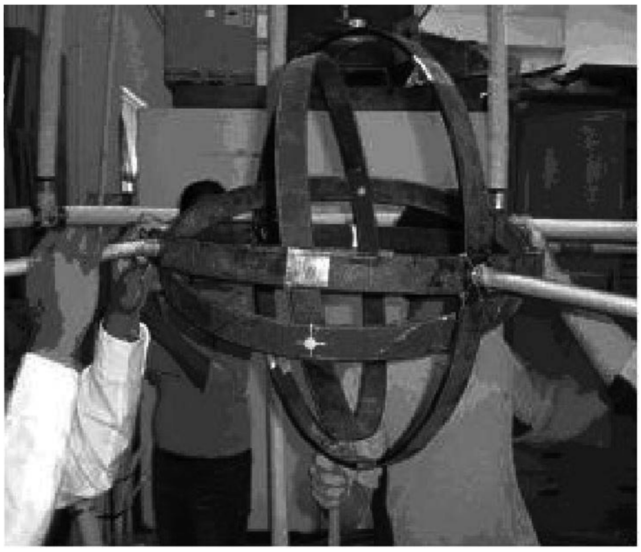

Fig. 16 TEDII double gimbal system (DGS).

3. *Tumbleweed Earth Demonstrator III*

The main purpose of the TEDIII was to improve upon the previous TED designs. The TEDIII outer structure was made of 1 1/2-in. schedule 40 PVC pipe, which allowed the TEDIII to remain adequately rigid. Two side rings were also added to better distribute the dynamic stress applied on the outer structure. These side rings were made of the same PVC pipe as the outer structure. The new PVC structure was formed by bending the PVC pipe to the correct radius using a special jig, heating the pipe using boiling water, and allowing it to cool while remaining in its deformed shape in the jig. The sail retraction and deployment system (SRDS), double gimbal, and MIS were also improved from the previous TED design. The SRDS was modified to retract almost 100% of the sail and deploy it to its original position remotely. Therefore, the TEDIII could be stopped and started by retracting and deploying the sails, respectively. The DGS was redesigned, made of stainless steel, with an extra ring added for structural support. Figure 18 shows the completed TEDIII with the SRDS, DGS, and MIS incorporated.

C. Testing

The first TEDIII test, seen in Fig. 19, was conducted at Nags Head Beach, North Carolina. Three TEDIIIs were constructed on site with only the outer structure, struts, and fixed sails. The purpose of this test was to place the TEDs in different positions along the beach and observe the group behavior. Wind speeds during testing were variable and inconsistent, but we were able to make some qualitative observations. First we observed that a 30-ft/s gust of wind would initiate rolling and a constant 20-ft/s wind was needed to maintain rolling (both numbers are approximate). We also noticed that the TEDs had considerable effect on each other. When one TED was

Fig. 17 Tumbleweed Earth Demonstrator II.

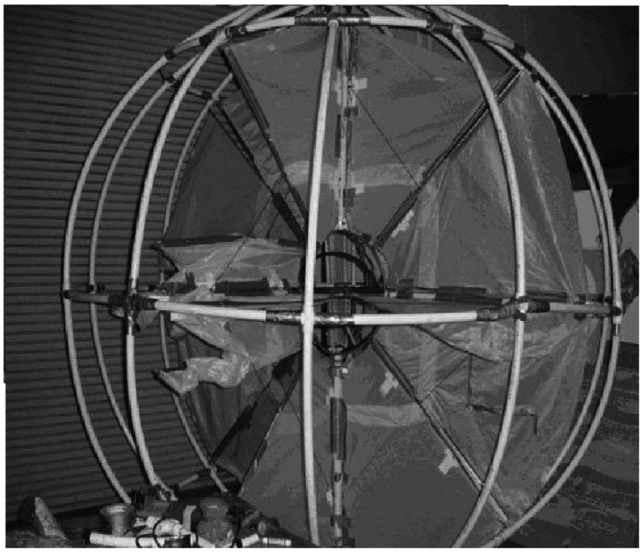

Fig. 18 Tumbleweed Earth Demonstrator III.

directly upwind of the others, the airflow was disrupted and prevented any movement of the others. This effect varied with the wind speed and the distance between the TEDs. If the TEDs were beside one another and separated by a few feet, the rolling motion was unaffected. However, if the TEDs were too close to each other at initial rolling, they would follow similar paths and ultimately one would block the airflow of the others.

A significant observation was that of the vortex that was produced by the TED. Observations were made using streamers to determine the downstream effects of the TED, while conducting a static test with the TED anchored on blocks. Approximately 6 ft directly downstream of the TED, the wind was blowing back toward the stationary TED. This is consistent with the wake created downstream of a sphere. Further tests were conducted to map this vortex effect. It was found that the air began to curl back toward the TED from around 12–15 ft downwind. The mapped effect was cone shaped, with the wider area forming at the outer edges of the TED. This led to the idea of perforating the sails to create a lower backpressure and increase drag while counteracting the vortex.

Fig. 19 Three Tumbleweed Earth Demonstrator IIIs on the beach during testing.

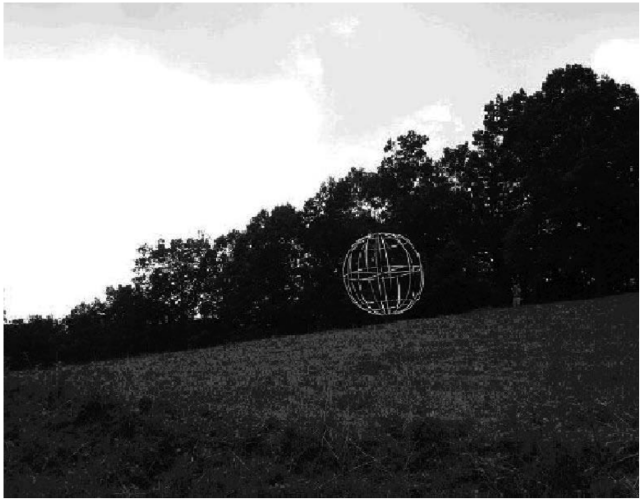

Fig. 20 Tumbleweed Earth Demonstrator III bouncing during mountain testing.

The second set of tests were conducted in the mountains of Lake Toxaway, North Carolina. The purpose of this test was to determine the TEDIII's ability to navigate rough terrain, found in canyons or ravines. This test was inspired by the need to know more about the possible failure modes of tumbleweed rovers, such as getting stuck on rocks and physical failure due to impact. A single TEDIII was constructed with only the outer structure and struts and rolled down a steep ravine. Obstructions of varying heights were placed in the path of the TEDIII. The results showed a TEDIII could overcome obstructions almost half of its diameter. Some structural failures occurred, when the PVC joints sheared due to repeated impacts. However, none of these failures seemed to significantly impede the rolling motion of the TEDIII. This differed from the TEDII, which stopped rolling when the structure failed.

TEDIII was also tested on a mountainous pasture. It became evident from this test that the TEDIII could develop a significant bounce, seen in Fig. 20, when rolling down a steep slope and encountering terrain variations, before the bounce damped out and it started to roll normally. During these test runs, more damage occurred to the structure and one of the main members separated from the hub. Still this failure had no appreciable affect on the TED's rolling motion [17].

D. Discussion of Tumbleweed Earth Demonstrator Design

Throughout the design, manufacturing and testing of the Mars Tumbleweed Earth Demonstrator, many interesting characteristics

and behaviors were observed. Beginning with the TEDI, design flaws were evident after construction and testing, resulting in the TEDII, and ultimately the TEDIII.

The Tumbleweed Earth Demonstrator III consists of a semirigid outer structure, orthogonal sails, a sail retraction and deployment system, and a double gimbaled modular instrument system. The Tumbleweed Earth Demonstrator III was tested over varying terrain. During TEDIII beach testing it was found that when grouped together one TED will affect the airflow over the others and impede their rolling motion. Vortices were also discovered in the wake of the TEDIII; this led to the idea of introducing sail perforations to create a lower backpressure and hence increase drag to counteract these vortices. During Tumbleweed Earth Demonstrator III mountain testing it was observed that a TEDIII could overcome obstacles up to half of its diameter in size and that minor structural failures had little to no effect on the TED's rolling motion.

IV. Modeling and Analysis of Potential Tumbleweed Navigation System

So far we have investigated different designs for using wind to propel a tumbleweed rover, but have not considered the issue of steering, or navigation. One possible technique for steering a tumbleweed involves varying the location of the center of mass to affect the direction of the tumbleweed as it is blown across the Martian terrain. Before designing a variable-center-of-mass navigational control system, it is first necessary to develop mathematical models of tumbleweed rolling dynamics and investigate how its rolling motion is affected by different locations of the center of mass. A survey of the literature on rolling dynamics reveals many interesting papers [18–45], but none of these address the issue of a rolling sphere with a variable center of mass location; therefore, in this section of the paper, we present such a mathematical model and perform computer simulations illustrating the dramatic effect that the center of mass location has on the motion of the tumbleweed rover.

A. Mathematical Model

Our basic approach will be to use Newton–Euler methods to derive equations of motion for the tumbleweed, and then to integrate these equations numerically. Setting the sum of the external forces and external torques acting on the tumbleweed equal to the acceleration of the center of mass of the tumbleweed and the time derivative of the angular momentum of the tumbleweed, respectively, yields six kinetic equations. We then use a standard set of kinematic relations to relate angular and linear velocities to the position and orientation of the tumbleweed. The most subtle part of the derivation involves dealing with the fact that the tumbleweed at times will slip and at other times will roll without slipping. Therefore, at each time step, it is assumed that no slipping occurs, and the no-slip condition (involving the coefficient of static friction) is tested. If the condition is met, then the no-slip assumption was correct, and we proceed to the next time step. However, if the condition is not met, then the time step is repeated using equations derived by assuming that slipping occurs. Assuming the tumbleweed is rolling along a flat surface while experiencing wind loading with components in the x, y, and z directions, we outline the derivation of our equations of motion next.

Consider the tumbleweed rover as a rigid body with a coordinate system embedded in the body with origin at B (the center of the sphere); this embedded coordinate system is denoted as $\{\mathbf{i}_B, \mathbf{j}_B, \mathbf{k}_B\}$. All positions are in reference to an inertial frame with origin O. Figure 21 shows a diagram of the tumbleweed with related reference frames. The external torques acting on the body are related to the rate of change of the angular momentum as follows:

$$\tau_{B,\text{sys}} = {}^{O}\frac{\mathrm{d}}{\mathrm{d}t}{}^{O}\mathbf{h}_{B,\text{sys}} + {}^{O}\mathbf{v}_{B/O} \times m_{\text{TOT}}{}^{O}\mathbf{v}_{\text{c.m.}/O} \tag{1}$$

where $\tau_{B,\text{sys}}$ is the sum of all external torques acting on the system about point B, ${}^{O}\frac{\mathrm{d}}{\mathrm{d}t}{}^{O}\mathbf{h}_{B,\text{sys}}$ is the time derivative with respect to the inertial frame of the angular momentum of the system about point B,

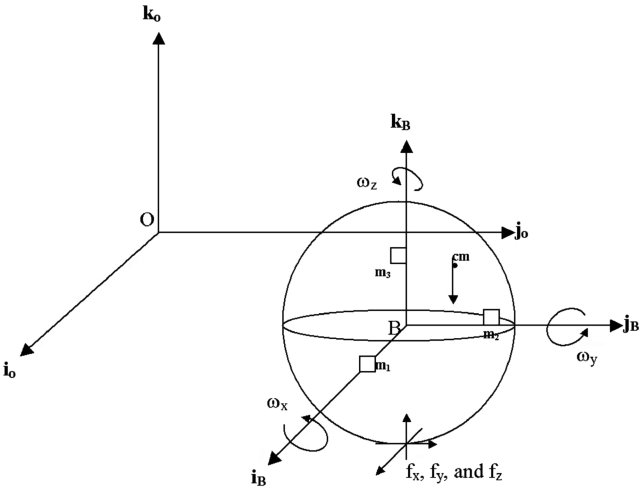

Fig. 21 Tumbleweed diagram with inertial and body reference frames.

${}^{O}\mathbf{v}_{B/O}$ is the velocity of point B with respect to the inertial frame, m_{TOT} is the total mass of the system, and ${}^{O}\mathbf{v}_{\text{c.m.}/O}$ is the velocity of the center of mass of the system with respect to the inertial frame. The sum of the external forces acting on the system is related to the acceleration of the center of mass of the system as follows:

$$\sum \mathbf{F} = m_{\text{TOT}}{}^{O}\mathbf{a}_{\text{c.m.}/O} \tag{2}$$

where $\sum \mathbf{F}$ is the sum of all external forces acting on the system and ${}^{O}\mathbf{a}_{\text{c.m.}/O}$ is the acceleration of the center of mass of the system with respect to the inertial frame. The full expansion of these terms is very lengthy and is not presented here, but can be found in Wilson's thesis [46].

B. Simulations

We now show how our equations of motion can be used to investigate the effect of varying the location of the center of mass of the tumbleweed on its motion. The following simulations are for a 6.6-ft diam tumbleweed propelled along a flat Martian surface by a constant wind loading. The wind force is arbitrarily chosen to be a 0.9-lb force in the x direction and is assumed to be constant, because for the time duration observed, the velocity of the tumbleweed is significantly less than the wind speed. Mass distributions and initial angular velocities are varied for 12 different cases as shown in Table 2. Figures 22–33 show the trajectories of the tumbleweed in the x_0–y_0 plane for the various parameter values and initial conditions shown in Table 2. The parameters and variables listed in Table 2 are defined as follows: m_{1_A}, m_{2_A}, and m_{3_A} are small submasses located along the $\mathbf{i}_B$, $\mathbf{j}_B$, and $\mathbf{k}_B$ axes, respectively, as shown in Fig. 21; m_{1_B}, m_{2_B}, and m_{3_B} are small submasses, located along the negative $\mathbf{i}_B$, $\mathbf{j}_B$, and $\mathbf{k}_B$ axes, respectively; x_{1_A}, x_{1_B}, y_{2_A}, y_{2_B}, z_{3_A}, and z_{3_B} are the distances from the center of mass of the system to the m_{1_A}, m_{1_B}, m_{2_A}, m_{2_B}, m_{3_A}, and m_{3_B} submasses, respectively; and ω_x, ω_y, and ω_z are the initial angular velocities of the tumbleweed rover about the $\mathbf{i}_B$, $\mathbf{j}_B$, and $\mathbf{k}_B$ axes, respectively. The numerical scheme used to integrate the equations of motion was a Dormand–Prince 4(5) pair (MATLAB's ode45).

C. Discussion of Results

For the 12 different cases shown in Figs. 22–33, we see that the mass imbalance, wind force, and initial angular velocity all affect the motion of the tumbleweed. We next discuss each of the individual cases.

1) Case 1 (Fig. 22): For case 1, the tumbleweed is balanced and has an initial angular velocity about the x axis. Thus the tumbleweed first rolls in the negative y direction, but the wind force then causes it to roll in the x direction.

Table 2 Parameter values and initial conditions for tumbleweed simulations (masses are in pounds mass, distances are in feet, and angular velocities are in radians per second)

	m_{1_A}	m_{1_B}	m_{2_A}	m_{2_B}	m_{3_A}	m_{3_B}	x_{1_A}	x_{1_B}	y_{2_A}	y_{2_B}	z_{3_A}	z_{3_B}	w_x	w_y	w_z
Case 1	5.5	5.5	5.5	5.5	5.5	5.5	0.33	−0.33	0.33	−0.33	0.33	−0.33	0.5	0	0
Case 2	5.5	5.5	5.5	5.5	5.5	5.5	0.33	−0.33	0.33	−0.33	0.33	−0.33	0	0.5	0
Case 3	11	5.5	5.5	5.5	5.5	5.5	1.65	−0.33	0.33	−0.33	0.33	−0.33	0.5	0	0
Case 4	11	5.5	5.5	5.5	5.5	5.5	1.65	−0.33	0.33	−0.33	0.33	−0.33	0	0.5	0
Case 5	5.5	5.5	11	5.5	5.5	5.5	0.33	−0.33	1.65	−0.33	0.33	−0.33	0.5	0	0
Case 6	5.5	5.5	11	5.5	5.5	5.5	0.33	−0.33	1.65	−0.33	0.33	−0.33	0	0.5	0
Case 7	5.5	5.5	5.5	5.5	11	5.5	0.33	−0.33	0.33	−0.33	1.65	-0.33	0.5	0	0
Case 8	5.5	5.5	5.5	5.5	11	5.5	0.33	−0.33	0.33	−0.33	1.65	−0.33	0	0.5	0
Case 9	11	5.5	5.5	5.5	5.5	5.5	3.3	−0.33	0.33	−0.33	0.33	−0.33	0.5	0	0
Case 10	11	5.5	5.5	5.5	5.5	5.5	3.3	−0.33	0.33	−0.33	0.33	−0.33	0	0.5	0
Case 11	5.5	5.5	11	5.5	5.5	5.5	0.33	−0.33	3.3	−0.33	0.33	−0.33	0.5	0	0
Case 12	5.5	5.5	11	5.5	5.5	5.5	0.33	−0.33	3.3	−0.33	0.33	−0.33	0	0.5	0

2) Case 2 (Fig. 23): For case 2, the tumbleweed is balanced and has an initial angular velocity about the y axis. Thus the tumbleweed begins rolling in the positive x direction and the wind force maintains this rolling in the x direction.

3) Case 3 (Fig. 24): For case 3, the tumbleweed is imbalanced along the x axis and has an initial angular velocity about the x axis. Thus the tumbleweed first rolls in the negative y direction, but the mass imbalance causes the tumbleweed to begin rolling in the positive y direction.

4) Case 4 (Fig. 25): For case 4, the tumbleweed is imbalanced along the x axis and has an initial angular velocity about the y axis. Thus the tumbleweed begins rolling in the positive x direction and the wind force maintains this rolling in the x direction.

5) Case 5 (Fig. 26): For case 5, the tumbleweed is imbalanced along the y axis and has an initial angular velocity about the x axis. Thus the tumbleweed first rolls in the negative y direction, but the mass imbalance causes the tumbleweed to begin rolling in the positive y direction.

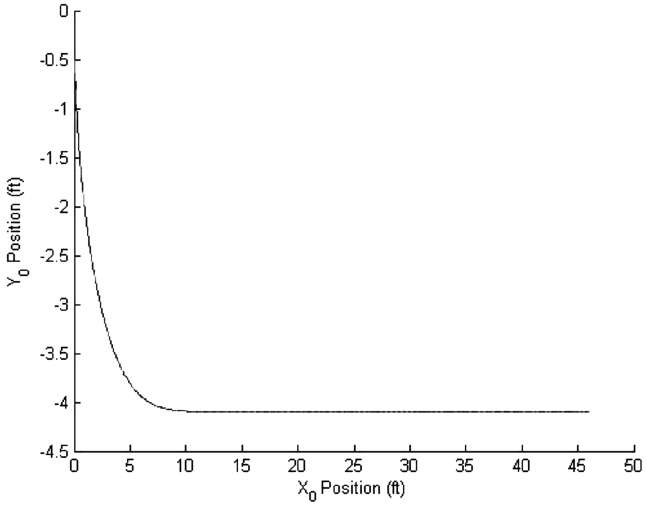

Fig. 22 Case 1 model simulation.

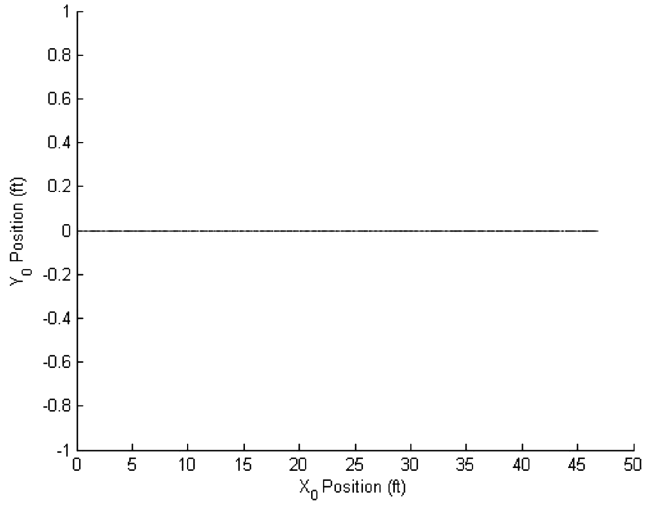

Fig. 23 Case 2 model simulation.

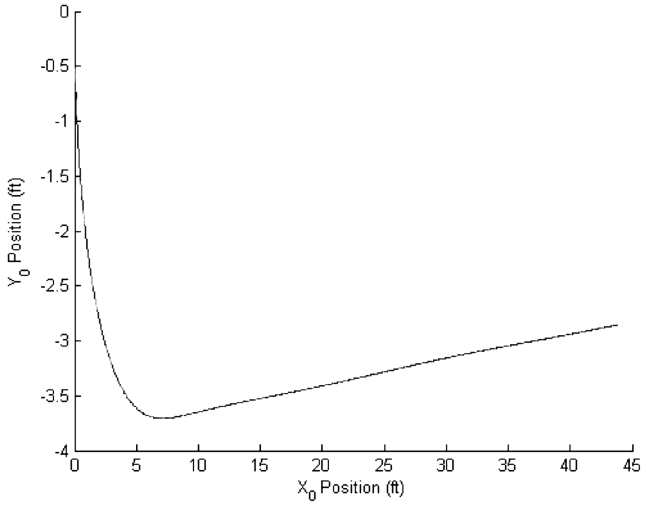

Fig. 24 Case 3 model simulation.

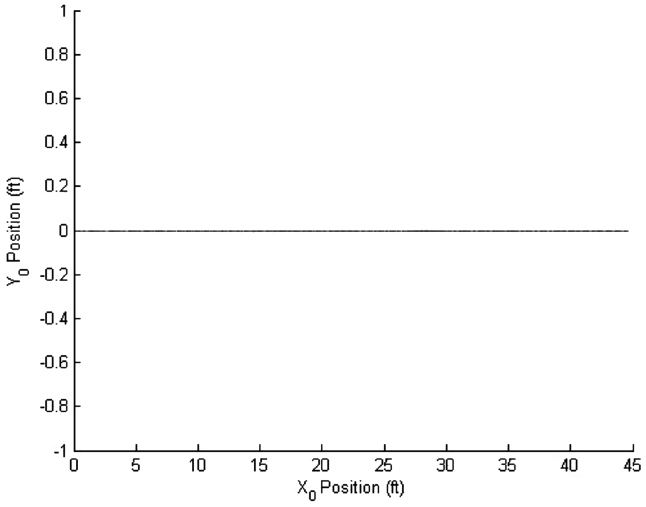

Fig. 25 Case 4 model simulation.

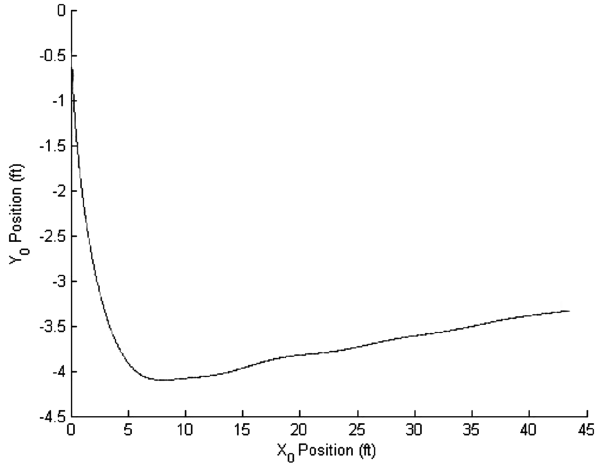

Fig. 26 Case 5 model simulation.

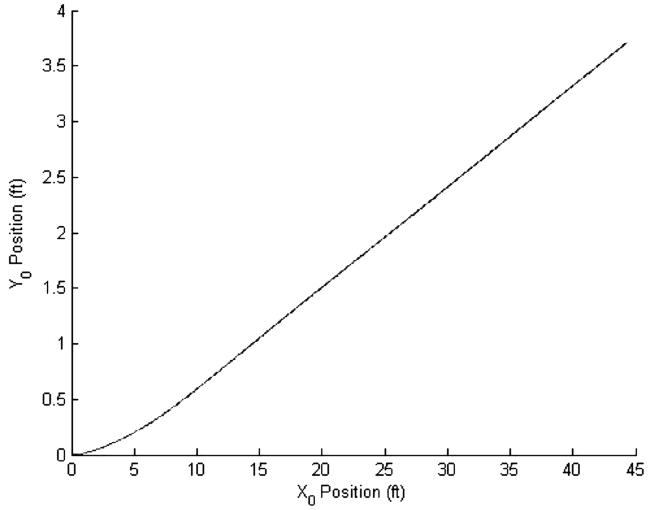

Fig. 27 Case 6 model simulation.

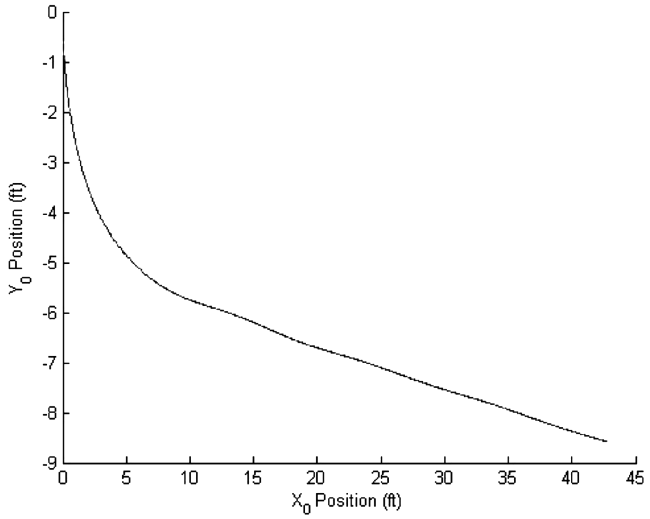

Fig. 28 Case 7 model simulation.

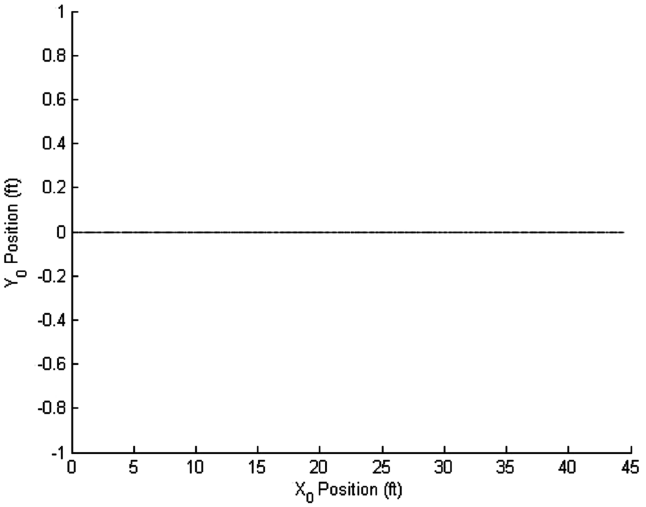

Fig. 29 Case 8 model simulation.

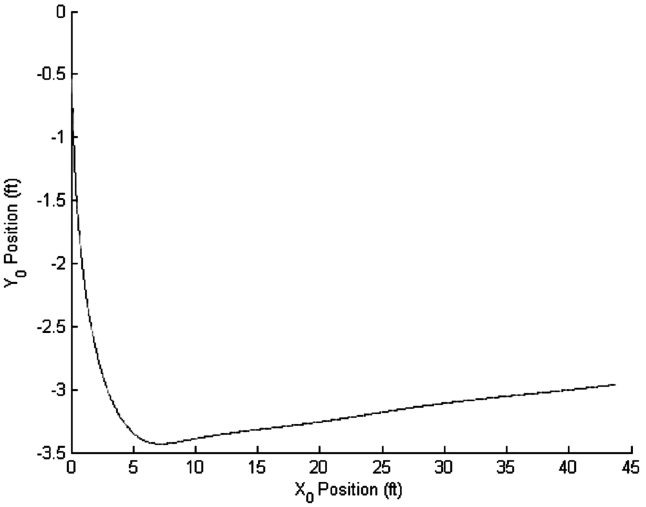

Fig. 30 Case 9 model simulation.

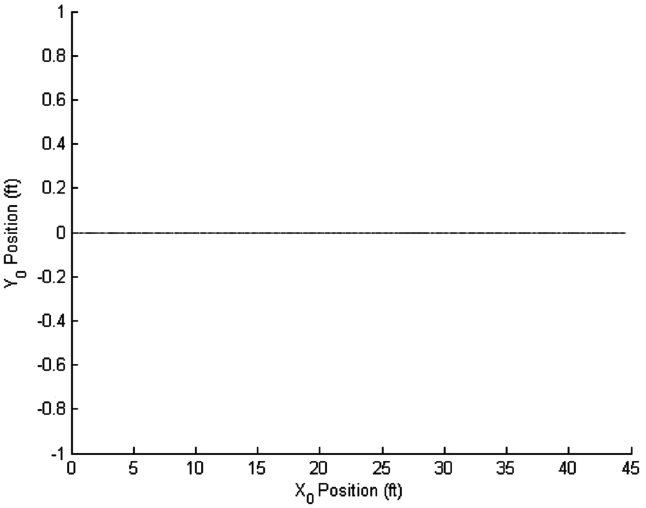

Fig. 31 Case 10 model simulation.

6) Case 6 (Fig. 27): For case 6, the tumbleweed is imbalanced along the *y* axis and has an initial angular velocity about the *y* axis. The initial velocity as well as the wind force causes the tumbleweed to roll in the positive *x* direction, however, the mass imbalance along the positive *y* axis causes the tumbleweed to roll in the positive *y* direction. These effects happen simultaneously leading to the trajectory shown in the figure.

7) Case 7 (Fig. 28): For case 7, the tumbleweed is experiencing a mass imbalance along the *z* axis and has an initial angular velocity about the *x* axis. The initial angular velocity causes the tumbleweed

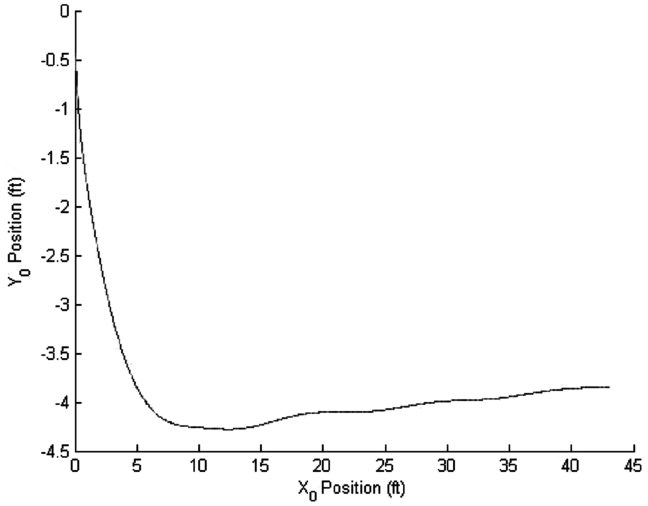

Fig. 32 Case 11 model simulation.

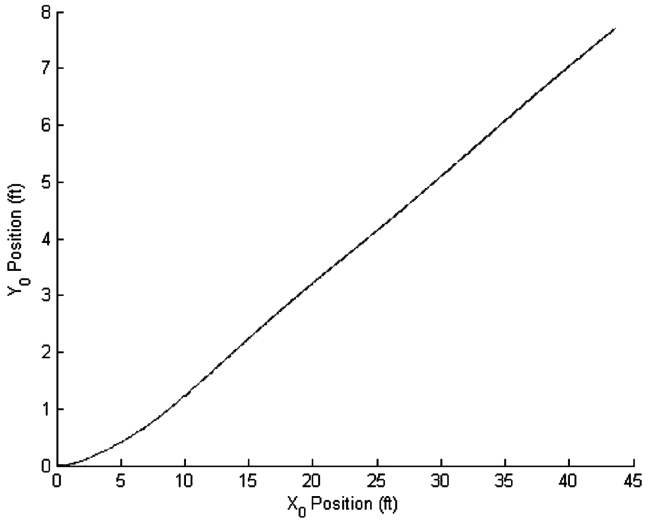

Fig. 33 Case 12 model simulation.

to roll in the negative *y* direction and the wind force causes it to roll in the positive *x* direction. The mass imbalance along the *z* axis causes the tumbleweed to continue rolling in the negative *y* direction.

8) Case 8 (Fig. 29): For case 8, the tumbleweed is imbalanced along the *z* axis and has an initial angular velocity about the *y* axis. This angular velocity causes the tumbleweed to begin rolling in the positive *x* direction and the mass imbalance and wind force maintains this rolling in the *x* direction.

9) Case 9 (Fig. 30): For case 9, the tumbleweed is imbalanced along the *x* axis and has an initial angular velocity about the *x* axis which causes the tumbleweed to first roll in the negative *y* direction. The mass imbalance, however, causes the tumbleweed to begin rolling in the positive *y* direction.

10) Case 10 (Fig. 31): For case 10, the tumbleweed is imbalanced along the *x* axis and has an initial angular velocity about the *y* axis which causes the tumbleweed to begin rolling in the positive *x* direction and the wind force maintains this rolling in the *x* direction.

11) Case 11 (Fig. 32): For case 11, the tumbleweed is imbalanced along the *y* axis and has an initial angular velocity about the *x* axis which causes the tumbleweed to first roll in the negative *y* direction. The mass imbalance, however, causes the tumbleweed to begin rolling in the positive *y* direction.

12) Case 12 (Fig. 33): For case 12, the tumbleweed is imbalanced along the *y* axis and has an initial angular velocity about the *y* axis. The initial velocity as well as the wind force causes the tumbleweed to roll in the positive *x* direction; however, the mass imbalance along the positive *y* axis causes the tumbleweed to roll in the positive *y* direction. These effects happen simultaneously leading to the trajectory shown in the figure.

As discussed previously, Figs. 22–33 show that by varying the location of the center of mass, the motion of the tumbleweed rover can be significantly affected, indicating that a navigation system based on dynamically changing the center of mass of the tumbleweed comprises a promising area of research and development. The next step in developing a viable navigation system based on this phenomenon would be to develop control algorithms designed to dynamically alter the location of the center of mass of the rover (e.g., via a set of orthogonally placed screw drives which can quickly move masses toward or away from the center of the rover) to cause the rover to trace out a desired path. In this paper, our simulations concern rovers with different center of mass locations, but the location of the center of mass does not vary during the course of the simulations. The equations presented in this paper and in Wilson's thesis [46] do account for a time varying center of mass, however, and provide the basis for designing a navigation system based on dynamically changing the center of mass of the rover.

V. Summary

From wind-tunnel tests conducted on different tumbleweed rover designs, we have shown that a box-kite configuration represents a promising design for a Mars Tumbleweed rover. To aid in the development of such a rover, three generations of a Tumbleweed Earth Demonstrator based on the box-kite concept have been designed, constructed, and tested. These Earth demonstrators represent an important first step in developing viable Mars Tumbleweed rovers. Finally, a possible method for steering a Mars Tumbleweed rover has been identified, namely, using a system of moving masses within the tumbleweed to alter the location of the center of mass. A mathematical model of such a system has been developed and simulated, and it has been demonstrated that such a system has the potential to form the basis of a navigation system for Mars Tumbleweed rovers, that is, the results show that it is possible to dramatically alter the path of a tumbleweed rover by shifting its center of mass.

Acknowledgments

The authors gratefully acknowledge support from the National Institute of Aerospace and the North Carolina Space Grant Consortium. The authors would like to thank Dennis Bushnell and the NASA Langley Research Center (LaRC) Creativity & Innovation (C&I) initiative and Rich Antcliff and the LaRC Innovation Institute (ii) for their support of tumbleweed research. The authors would also like to thank Philip Calhoun, Steve Bauer, and Steven Harris, members of the NASA LaRC Tumbleweed team who assisted with the test, and Luther Jenkins and Richard White, for their operation of the NASA Langley Research Center Basic Aerodynamic Research Tunnel (BART) facility.

References

[1] Lorenz, R. D., *Spinning Flight: Dynamics of Frisbees, Boomerangs, Samaras, and Skipping Stones*, Springer, New York, 2006, pp. 60–66.

[2] Jones, J., and Yavrouian, A., "Lightweight "Beach-Ball Robotic Vehicles," NASA Technical Brief, Jet Propulsion Laboratory New Technology, Rept. 9894-20283, Jet Propulsion Laboratory Technology Reporting Office, 1997.

[3] Wang, H., Yang, B., and Jones, J. A., "Mobility Analysis of an Inflated Tumbleweed Ball Under Wind Loads," AIAA Paper 2002-1556, April 2002.

[4] Lorenz, R. D., Jones, J. A., and Wu, J. J. "Mars Magnetometry from a Tumbleweed Rover," *Aerospace Conference*, IEEE, Piscataway, NJ, Vol. 2, March 2003, pp. 597–602.

[5] Kuhlman, K. R., Behar, A. E., Jones, J. A., Carsey, F., Hajos, G. A., Flick, J. J., and Antol, J., "Tumbleweed: A New Paradigm for Surveying the Surface of Mars for In-Situ Resources," *Space Resources Roundtable VI*, Colorado School of Mines, the Lunar and Planetary Institute, and the Space Resources Roundtable, Inc., Golden, CO, Nov. 2004, p. 27.

[6] Antol, J., Woodward, S. E., Hajos, G. A., Heldmann, J. L., and Taylor, B. D., "Using Wind Driven Tumbleweed Rovers to Explore Martian Gully Features," AIAA Paper 2002-0245, Jan. 2005.
[7] Hajos, G. A., Jones, J. A., Behar, A., and Dodd, M., "An Overview of Wind-Driven Rovers for Planetary Exploration," AIAA Paper 2002-0244, Jan. 2005.
[8] Antol, J., "A New Vehicle for Planetary Surface Exploration: The Mars Tumbleweed," AIAA Paper 2002-2520, Jan. 2005.
[9] Behar, A., Carsey, F., Matthews, J., and Jones, J., "NASA/JPL Tumbleweed Polar Rover," *Aerospace Conference*, IEEE, Piscataway, NJ, Vol. 1, March 2004, pp. 388–395.
[10] Calhoun, P. C., Harris, S. B., Raiszadeh, B., and Zaleski, K. D., "Conceptual Design and Dynamics Testing and Modeling of a Mars Tumbleweed Rover," AIAA Paper 2005-0247, Jan. 2005.
[11] Flick, J. J., and Toniolo, M. D., "Preliminary Dynamic Feasibility and Analysis of a Spherical, Wind-Driven (Tumbleweed), Martian Rover," AIAA Paper 2005-0250, Jan. 2005.
[12] DeJarnette, F. R., Casper, K. M., Maxwell, B. K., Schwarz, J. B., Sebastian, T., Engler, W. O., III, Hanrahan, H. C., and Lam, N. T., "Deployment Devices and Solar Power for Mars Tumbleweed Rovers," AIAA Paper 2005-0246, Jan. 2005.
[13] Antol, J., Hajos, G. A., and Strickland, C., "Wind Tunnel Tests of Evolved Mars Tumbleweed Concepts," AIAA Paper 2006-0069, Jan. 2006.
[14] James, D. L., Rose, S. E., Moody, C. B., and Barhorst, A., "Drag Measurement and Dynamic Simulation of Martian Wind Driven Sensor Platform Concepts," AIAA Paper 2005-0249, Jan. 2005.
[15] Jones, J., and White, C., "Tumbleweed Materials and Structures Study-A Final Report of a JPL Study for Langley Research Center," Jet Propulsion Laboratory, California Institute of Technology, March 2004.
[16] Strickland, C. V., and Keyes, J. P., "Wind Tunnel Tests to Determine Drag Coefficients for the Mars Tumbleweed," AIAA Paper 2005-0248, Jan. 2005.
[17] Claycomb, J. S., DeJarnette, F. R., and Mazzoleni, A. P. "Development and Construction of a Prototype Mars Tumbleweed Rover," AIAA Paper 2006-0066, Jan. 2006.
[18] Kilin, A. A., "The Dynamics of Chaplygin Ball: The Qualitative and Computer Analysis," *Regular and Chaotic Dynamics Journal* [online journal], Vol. 6, No. 2, 2001, pp. 291–306, http://dx.doi.org/10.1070/RD2001v006n03ABEH000178 [retrieved 20 June 2006].
[19] Duistermaat, J. J., "Chaplygin's Sphere," ArXiv Mathematics e-prints [online], Sept. 2004, http://adsabs.harvard.edu/abs/2004math.....9019D [retrieved 20 June 2006].
[20] Cantrijin, F., de Leon, M., and Martin de Diego, D., "On Almost-Poisson Structures in Nonholonomic Mechanics," *Nonlinearity Journal* [online journal], Vol. 12, No. 3, 1999, pp. 721–737, http://dx.doi.org/10.1088/0951-7715/12/3/316 [retrieved 20 June 2006].
[21] Schneider, D., "Non-Holonomic Euler-Poincare Equations and Stability in Chaplygin's Sphere," *Dynamical Systems* [online journal], Vol. 17, No. 2, June 2002, pp. 87–130, http://www.ingentaconnect.-com/content/tandf/cdss/2002/00000017/00000002/art00001.
[22] Abdelkader, M. A., "Ball Rolling on an Rotating Plane," *Zeitschrift fuer Angewandte Mathematik und Mechanik*, Vol. 66, No. 11, 1986, pp. 563–564. doi:10.1002/zamm.19860661117
[23] Holden, J. T., and King, A. C., "The Dynamics of a Ball Rolling on a Rotating Plane," *Zeitschrift fur Angewandte Mathematik und Mechanik*, Vol. 70, No. 8, 1990, pp. 353–355. doi:10.1002/zamm.19900700825
[24] Borisov, A. V., and Mamaev, I. S., "Motion of Chaplygin Ball on an Inclined Plane," *Doklady Physics* [online journal], Vol. 51, No. 2, Feb. 2006, pp. 73–76, http://dx.doi.org/10.1134/S1028335806020078 [retrieved 20 June 2006]. doi:10.1134/S1028335806020078
[25] Zav'yalov, O. G., and Markov, Y. G., "Study of the Dynamics of a Sphere Rolling Over the Surface with an Unsteady Viscous Fluid Layer," *Trenie i Iznos*, Vol. 23, No. 2, 2002, pp. 120–129.
[26] Fufaev, N. A., "Theory of the Motion of Systems with Rolling," *Applied Mathematics and Mechanics* (English translation of *Prikladnaya Matematika i Mekhanika*) [online journal], Vol. 49, No. 1, 1985, pp. 41–49, http://dx.doi.org/10.1016/0021-8928(85)90124-8 [retrieved 20 June 2006].
[27] Liu, Y. Z., "On the Motion of an Asymmetrical Rigid Body Rolling on a Horizontal Plane," *Zeitschrift fuer Angewandte Mathematik und Mechanik*, Vol. 65, No. 3, 1985, pp. 180–183. doi:10.1002/zamm.19850650314
[28] Sato, O., Shimojima, H., Saito, A., and Kaneko, T., "Dynamic and Static Characteristics of Rolling Rigid Bodies," *Bulletin of the Japan Society of Mechanical Engineers*, Vol. 29, No. 258, 1986, pp. 4375–4380.
[29] Hu, P. H., and Ehmann, K. F., "Dynamic Model of the Rolling Process. Part 2: Inhomogeneous Model," *International Journal of Machine Tools and Manufacture* [online journal], Vol. 40, No. 1, 2000, pp. 21–31, http://dx.doi.org/10.1016/S0890-6955(99)00050-4 [retrieved 20 June 2006]. doi:10.1016/S0890-6955(99)00050-4
[30] Bicchi, A., Balluchi, A., Prattichizzo, D., and Gorelli, A., "Introducing the "SPHERICLE": An Experimental Testbed for Research and Teaching in Nonholonomy," *International Conference on Robotics and Automation*, Vol. 3, IEEE, Piscataway, NJ, April 1997, pp. 2620–2625.
[31] Bicchi, A., Chitour, Y., and Marigo, A., "Reachability and Steering of Rolling Polyhedra: A Case Study in Discrete Nonholonomy," *IEEE Transactions on Automatic Control* [online journal], Vol. 49, No. 5, 2004, pp. 710–726, http://dx.doi.org/10.1109/TAC.2004.826727 [retrieved 20 June 2006]. doi:10.1109/TAC.2004.826727
[32] Kuleshov, A. S., "First Integrals in the Problem of Rolling a Body of Revolution Over a Rough Plane," *Doklady Physics* [online journal], Vol. 48, No. 7, 2003, pp. 385–387, http://dx.doi.org/10.1134/1.1598254 [retrieved 20 June 2006]. doi:10.1134/1.1598254
[33] Salazar, A., and Sanchez-Lavega, A., "Motion of a Ball on a Rough Horizontal Surface After Being Stuck by a Tapering Rod," *European Journal of Physics* [online journal], Vol. 11, No. 4, 1990, pp. 228–232, http://dx.doi.org/10.1088/0143-0807/11/4/006 [retrieved 20 June 2006]. doi:10.1088/0143-0807/11/4/006
[34] Kuleshov, A. S., "On Steady Rolling of a Disk on the Rough Plane," *Prikladnaya Matematika i Mekhanika*, Vol. 65, No. 1, 2001, pp. 173–175.
[35] Chigarev, A. V., Tsyganov, A. R., and Kuz'mitskij, A. V., "Influence of the Wave Effect on the Dynamics of Rolling Friction of a Wheel," *Trenie i Iznos*, Vol. 22, No. 1, 2001, pp. 51–57.
[36] Fedorov, Y. N., "Rolling of a Disk Over an Absolutely Rough Surface," *Mechanics of Solids* (English translation of *Izvestiya Akademii Nauk SSSR, Mekhanika Tverdogo Tela*), Vol. 22, No. 4, 1987, pp. 65–73.
[37] Le Saux, C., Leine, R. I., and Glocker, C., "Dynamics of a Rolling Disk in the Presence of Dry Friction," *Journal of Nonlinear Science* [online journal], Vol. 15, No. 1, 2005, pp. 27–61, http://dx.doi.org/10.1007/s00332-004-0655-4 [retrieved 20 June 2006]. doi:10.1007/s00332-004-0655-4
[38] Epstein, M., and Defaz, R. I., "The Pseudo-Rigid Rolling Coin," *Journal of Applied Mechanics* [online journal], Vol. 72, No. 5, 2005, pp. 695–704, http://dx.doi.org/10.1115/1.1979515 [retrieved 20 June 2006]. doi:10.1115/1.1979515
[39] Kolesnikov, S. N., "Rolling of a Disk Along a Horizontal Plane," *Moscow University mechanics bulletin* (English Translation of *Vestnik Moskovskogo Universiteta, Mek*, Vol. 40, No. 2, 1985, pp. 22–28.
[40] O'Reilly, O. M., "Dynamics of Rolling Disks and Sliding Disks," *Nonlinear Dynamics*, Vol. 10, No. 3, 1996, pp. 287–305. doi:10.1007/BF00045108
[41] Dahl, P. R., "A Solid Friction Model," Aerospace Corporation TOR-0158(3107-18)-1, El Segundo, CA, May 1968, http://handle.dtic.mil/100.2/ADA041920 [retrieved 20 June 2006].
[42] Huston, R. L., Passerello, C., Winget, J. M., and Sears, J., "On the Dynamics of a Weighted Bowling Ball," *Journal of Applied Mechanics*, Transactions ASME, , Vol. 46, No. 4, 1979, pp. 937–943.
[43] Al-Bender, F., and Symens, W., "Characterisation of Pre-Sliding and Pre-Rolling Friction," *Proceedings of the World Tribology Congress III—2005*, American Society of Mechanical Engineers, Fairfield, NJ, 2005, pp. 297–298.
[44] Terumichi, Y., Suda, Y., and Sogabe, K, "Dynamics of Rolling Wheel with Contact Rigidity and Slip," *ASME Design Engineering Technical Conference*, American Society of Mechanical Engineers, Fairfield, NJ, Sept. 2001, pp. 265–272.
[45] Sharma, N. L., and Reid, D. D., "Rolling as a Frictional Equilibration of Translation and Rotation," *European Journal of Physics* [online journal], Vol. 20, No. 3, 1999, pp. 129–136 [retrieved 20 June 2006], http://dx.doi.org/10.1088/0143-0807/20/3/001. doi:10.1088/0143-0807/20/3/001
[46] Wilson, J. L., "Design and Modeling of a Mars Tumbleweed Rover," M.S. Thesis, North Carolina State University, Department of Aerospace Engineering, Raleigh, NC, Dec. 2006.

David Spencer
Associate Editor